

Joint Neural SDF Reconstruction and Semantic Segmentation for CAD Models

Shen Fan¹✉ and Przemyslaw Musialski¹

New Jersey Institute of Technology, Newark NJ 07102, USA
{sf269, przem}@njit.edu

Abstract. We propose a simple, data-efficient pipeline that augments an implicit reconstruction network based on neural SDF-based CAD parts with a part-segmentation head trained under *PartField-generated* supervision. Unlike methods tied to fixed taxonomies, our model accepts *meshes with any number of parts* and produces coherent, geometry-aligned labels in a single pass. We evaluate on randomly sampled CAD meshes from the ABC dataset with intentionally varied part cardinalities—including over-segmented shapes—and report strong performance across reconstruction (CD_{L1}/CD_{L2} , $F1_{\mu}$, NC) and segmentation (mIoU, Accuracy), together with a new *Segmentation Consistency* metric that captures local label smoothness. We attach a lightweight segmentation head to the Flat-CAD SDF trunk; on a paired evaluation it does not alter reconstruction while providing accurate part labels for meshes with any number of parts. Even under degraded reconstructions on thin or intricate geometries, segmentation remains accurate and label-coherent, often preserving the correct part count. Our approach therefore offers a practical route to semantically structured CAD meshes without requiring curated taxonomies or exact palette matches. We discuss limitations in boundary precision—partly due to per-face supervision—and outline paths toward boundary-aware training and higher resolution labels.

Keywords: Semantic segmentation · CAD model · SDF reconstruction.

1 Introduction

Neural implicit fields, particularly signed distance functions (SDFs), are widely used to represent 3D geometry by encoding a surface as the zero-level set of a continuous neural function [16, 14, 22, 15]. This formulation provides resolution-independent evaluation and differentiable access to surface normals, and it has been adopted for reconstruction from point clouds and scans.

For computer-aided design (CAD) data, additional structure is required. CAD parts are predominantly composed of simple primitives (e.g., planes, cylinders, cones) and blends joined by sharp feature curves. Training with point-wise losses alone can yield surfaces that interpolate samples yet deviate from these structural regularities. Curvature-aware priors have therefore been introduced: the Implicit Geometric Regularizer (IGR) encourages unit-norm gradients [10]; DiGS penalizes divergence of the gradient field [3]; NeurCADRecon penalizes Gaussian curvature on a near-surface shell [7]; and Neural-Singular-Hessian constrains the Hessian near the surface [25]. More recent formulations reduce the cost of curvature regularization by targeting specific mixed second-

order terms while preserving geometric behavior [30], or specific activations for feature preservation [9].

A limitation of these approaches is that they focus on geometry without providing semantic part structure, which is often required in CAD workflows (e.g., for editing or downstream parametric recovery). Mesh-based pipelines can provide part labels, but they do not unify semantics with the implicit representation.

This work presents a joint implicit framework for CAD surface reconstruction and part segmentation. A shared neural backbone is paired with two output heads: one predicts SDF values trained with standard data, Eikonal, and curvature-regularization terms; the other predicts per-point semantic logits trained with a segmentation loss. This design allows querying both geometry and part labels in the same continuous 3D field. We also compare alternative segmentation-head designs (e.g., sine-activated and ReLU-based variants) and report their practical trade-offs.

Contributions. (i) A unified implicit formulation that combines curvature-regularized SDF reconstruction with per-part semantic labeling, and (ii) an empirical analysis of segmentation-head designs within this formulation, including the corresponding training objective and evaluation protocol on CAD models with part-level annotations.

2 Related Work

Implicit Neural Representations for 3D Shapes Neural implicit representations have revolutionized 3D shape modeling by encoding geometry as continuous functions. DeepSDF [16] pioneered learning signed distance functions with neural networks, while Occupancy Networks [14] used occupancy fields for shape representation. These foundational works demonstrated that MLPs could store complex geometries in a compact, differentiable form. Subsequent research has focused on improving reconstruction quality and efficiency. DiGS [3] introduces a divergence-guided shape representation for improved accuracy. GIFS [29] proposes a general implicit function for arbitrary shape topology. Points2Surf [8] learns implicit surfaces directly from raw point clouds without normals. For improved representation capacity, several works explore hierarchical and local approaches. Deep Local Shapes [4] learns a collection of local SDFs for detailed reconstruction. Convolutional Occupancy Networks [17] incorporates convolutional operations into implicit representations. IF-Net [6] uses multi-scale deep features for shape completion. These methods trade memory for improved detail capture.

CAD-Specific Neural Implicit Methods CAD models present unique challenges due to their precise geometric features, sharp edges, and planar surfaces. Standard implicit methods often struggle with these characteristics, motivating specialized approaches.

Neural-Singular-Hessian (NSH) [25] enforces singular Hessian constraints to preserve features in point cloud reconstruction. The method exploits the mathematical property that sharp edges correspond to singular points in the Hessian matrix. NeurCADRecon [7] explicitly targets zero Gaussian curvature regions common in manufactured objects, using specialized losses to encourage flat surfaces. FlatCAD [30] achieves the state-of-the-art in CAD reconstruction using an efficient curvature regularizer. FlatCAD’s key innovation is a proxy curvature term that encourages flat and cylindrical surfaces without expensive second-order derivative computation. Its SIREN backbone

makes it an ideal base for our joint segmentation-reconstruction approach. Other CAD-focused methods include Point2Cyl [24], which reverse-engineers 3D objects into extrusion cylinders, and various primitive-based approaches that decompose shapes into simple geometric elements. However, these methods typically require strong geometric priors that limit their generality.

3D Part Segmentation: From Manual to Automated Approaches While substantial progress has been made in 2D object part segmentation, the 3D counterpart has received less attention, in part due to the scarcity of annotated 3D datasets. 3D object part segmentation is essential for applications ranging from shape editing and retrieval to robotic manipulation and manufacturing. Traditional approaches relied on geometric cues [20], primitive fitting [19], or spectral clustering [21], but these methods struggle with complex, non-convex shapes.

Learning-based methods have shown promise but typically require extensive labeled data. PointNet [18] and its variants process point clouds directly but need category-specific training. BAE-NET [5] learns branched autoencoders for co-segmentation without part-level supervision but is limited to shapes with consistent structure. The lack of large-scale 3D part annotations remains a fundamental bottleneck.

Automated Part Annotation PartField [13] represents a significant advance in automated 3D part annotation. Unlike methods that rely on 2D projections or require category-specific training, PartField learns generalizable 3D feature fields that respect geometric boundaries. The method can decompose arbitrary meshes into semantically meaningful parts without manual annotation.

Critically, PartField’s ability to handle over-segmentation—producing more parts than strictly necessary—provides valuable robustness testing for downstream methods. By applying PartField to the ABC dataset, we create a scalable pipeline for generating part-level supervision without human intervention.

Joint Learning of Geometry and Semantics Several works explore joint learning of 3D geometry and semantics, though primarily for scene understanding rather than part segmentation. SurroundSDF [12] predicts both signed distance and semantic fields from surround-view images. ObjectSDF [26] and ObjectSDF++ [27] define per-object semantic fields for compositional scene representation. ClusteringSDF [28] fuses noisy 2D semantic predictions into consistent 3D representations.

For part-level understanding, PartSDF [23] outputs separate SDFs for each part but requires part annotations during training. Our work differs by learning a unified representation with a shared feature extractor, enabling more efficient inference and better feature sharing between geometry and semantics.

3 Method

3.1 Overview and Goals

We propose an extension of FlatCAD [30] that jointly learns surface reconstruction and semantic part segmentation from labeled point clouds. While FlatCAD excels at reconstructing flat geometric regions through its off-diagonal Weingarten loss formulation, it lacks the capability for semantic part segmentation. Our method introduces a

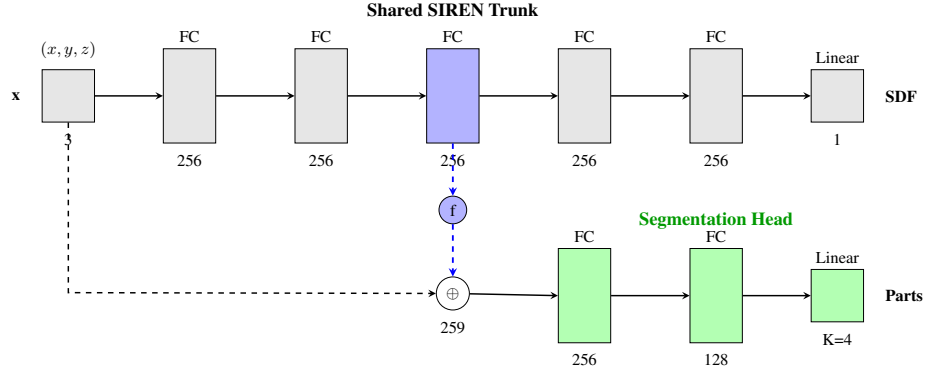


Fig. 1: Network architecture of the joint SDF-segmentation network. The shared SIREN trunk (5 layers, 256 neurons each) processes input coordinates through sine activations. Features are extracted from layer 3 (blue) and concatenated with input coordinates before being processed by a separate segmentation MLP (green). The original SDF prediction path remains unchanged from FlatCAD.

shared feature learning framework that leverages the geometric representations learned by FlatCAD’s SIREN network to simultaneously predict both signed distance values and part labels.

The key insight is that intermediate features learned for accurate surface reconstruction contain rich geometric information that can be effectively repurposed for semantic segmentation. By sharing the feature extraction backbone between tasks while maintaining separate prediction heads, we achieve:

1. Accurate surface reconstruction with flat regions (inherited from FlatCAD).
2. Consistent part segmentation that respects geometric boundaries.
3. Computational efficiency through shared feature extraction.
4. Minimal architectural overhead compared to the base FlatCAD model.

3.2 Network Architecture

Shared Feature Network As shown in Figure 1, the backbone is a five-layer SIREN [22]. The input layer maps \mathbb{R}^3 to \mathbb{R}^{256} with a sine activation of frequency $\omega_0 = 30$; four fully connected hidden layers of width 256 use sine activations with frequency $\omega = 1$. Denoting activations by ϕ_i ,

$$\phi_i(\mathbf{x}) = \begin{cases} \sin(\omega_0(\mathbf{W}_0\mathbf{x} + \mathbf{b}_0)), & i = 0, \\ \sin(\omega(\mathbf{W}_i\phi_{i-1} + \mathbf{b}_i)), & i \in \{1, 2, 3, 4\}. \end{cases}$$

We tap intermediate features at the third layer, $\mathbf{f} = \phi_2(\mathbf{x}) \in \mathbb{R}^{256}$, and reuse them in both heads. W_i and b_i denote learnable weights and biases of the i th fully connected layer.

Dual-Head Architecture SDF head. The reconstruction path continues with two sine layers and a linear projection

$$\begin{aligned}\phi_3(\mathbf{x}) &= \sin(\omega(\mathbf{W}_3\phi_2 + \mathbf{b}_3)), \\ \phi_4(\mathbf{x}) &= \sin(\omega(\mathbf{W}_4\phi_3 + \mathbf{b}_4)), \\ f(\mathbf{x}) &= \mathbf{W}_{\text{sdf}}\phi_4 + \mathbf{b}_{\text{sdf}}, \quad \mathbf{W}_{\text{sdf}} \in \mathbb{R}^{1 \times 256}.\end{aligned}$$

Segmentation head. The segmentation head is a simple three-layer MLP we designed. For part prediction we concatenate \mathbf{f} with the raw coordinates, $\mathbf{f}_{\text{seg}} = [\mathbf{f}; \mathbf{x}] \in \mathbb{R}^{259}$, and apply a three-layer MLP: $259 \rightarrow 256$ (ReLU, dropout $p = 0.2$), $256 \rightarrow 128$ (ReLU), and $128 \rightarrow K$ (linear logits; $K = 4$ in our experiments). This branch adds $\approx 10^5$ parameters (about 25% over a $\sim 4 \times 10^5$ backbone).

3.3 Joint Geometric and Segmentation Loss

We optimize a joint objective that combines geometric reconstruction terms with a semantic segmentation term. Let $\mathcal{X}_{\text{man}} = \{x_i\}_{i=1}^N$ denote on-surface (“manifold”) samples with available part labels on a subset $\mathcal{X}_{\text{lab}} \subseteq \mathcal{X}_{\text{man}}$, $\mathcal{X}_{\text{non}} = \{y_j\}_{j=1}^M$ denote uniform off-surface (“non-manifold”) samples, and $\Omega = \{p_\ell\}_{\ell=1}^L$ denote a thin near-surface shell used for curvature regularization. The network predicts a signed distance $f : \mathbb{R}^3 \rightarrow \mathbb{R}$ and part logits $\mathbf{g} : \mathbb{R}^3 \rightarrow \mathbb{R}^K$ (with K classes). The total loss is

$$\mathcal{L}_{\text{total}} = \lambda_{\text{DM}}\mathcal{L}_{\text{DM}} + \lambda_{\text{DNM}}\mathcal{L}_{\text{DNM}} + \lambda_{\text{EIK}}\mathcal{L}_{\text{EIK}} + \lambda_{\text{ODW}}\mathcal{L}_{\text{ODW}} + \lambda_{\text{SEG}}\mathcal{L}_{\text{SEG}}. \quad (1)$$

Manifold (Dirichlet) loss We pull on-surface samples to the zero level set [1]:

$$\mathcal{L}_{\text{DM}} = \frac{1}{N} \sum_{x \in \mathcal{X}_{\text{man}}} |f(x)|. \quad (2)$$

Non-manifold (sign-agnostic) loss For off-surface points we use a rapidly decaying sign-agnostic penalty (with $\alpha = 100$) [2]:

$$\mathcal{L}_{\text{DNM}} = \frac{1}{M} \sum_{y \in \mathcal{X}_{\text{non}}} \exp(-\alpha |f(y)|). \quad (3)$$

Eikonal loss. We regularize the field to satisfy the unit-gradient property of signed distances [10]:

$$\mathcal{L}_{\text{EIK}} = \frac{1}{K_e} \sum_{z \in \mathcal{Z}} \left(\|\nabla f(z)\|_2^2 - 1 \right)^2, \quad (4)$$

where \mathcal{Z} is a set of points sampled over the entire domain, and $K_e = |\mathcal{Z}|$.

Curvature gap loss. The off-diagonal Weingarten loss [30], which uses shell samples $p \in \Omega$, where $n = \nabla f(p) / \|\nabla f(p)\|$ and (u, v) form an orthonormal tangent frame at p (any rotation in the tangent plane is admissible) preserves flat regions. The off-diagonal entry of the Weingarten map in this frame is

$$S_{12}(p) = \frac{u^\top H_f(p) v}{\|\nabla f(p)\|_2},$$

where H_f is the Hessian of f . We penalize its magnitude to suppress the curvature gap:

$$\mathcal{L}_{\text{ODW}} = \frac{1}{L} \sum_{p \in \Omega} |S_{12}(p)|. \quad (5)$$

In practice, $S_{12}(p)$ is evaluated off-surface on the shell for numerical stability; either a Hessian–vector product or a symmetric finite-difference stencil may be used to obtain $u^\top H_f(p) v$ as proposed in [30].

Segmentation loss. For labeled manifold samples $x \in \mathcal{X}_{\text{lab}}$ with ground-truth part label $y(x) \in \{1, \dots, K\}$, we apply cross-entropy (CE) on the logits $\mathbf{g}(x)$:

$$\mathcal{L}_{\text{SEG}} = \frac{1}{|\mathcal{X}_{\text{lab}}|} \sum_{x \in \mathcal{X}_{\text{lab}}} \text{CE}(\text{softmax}(\mathbf{g}(x)), y(x)). \quad (6)$$

No segmentation loss is applied to unlabeled points.

3.4 Implementation Details

Inputs and outputs. We applied a pretrained PartField model to the ABC dataset [11] to produce per-face cluster IDs (visualized as colors) and exported both the colorized mesh and the per-face label array as ground-truth labels for training. From each ground-truth mesh we sample 30,000 surface points with associated part labels. Each iteration draws 20,000 on-surface (manifold) samples, 20,000 uniform off-surface (non-manifold) samples, and a thin near-surface shell used by the curvature regularizer. The network ingests 3D coordinates (and labels when present) and predicts SDF values for all points and K -way logits for labeled manifold points.

Curvature regularization and notation. We use the FlatCAD curvature-gap loss (off-diagonal Weingarten loss) on the near-surface shell. In the objective its weight is denoted λ_{ODW} (value 10 in our runs), matching our code and tables.

Initialization. Sine layers follow SIREN initialization: input weights $\mathbf{W}_0 \sim \mathcal{U}(-1/d, 1/d)$ (uniform sampling) for input dimension d (subsequent sine layers scaled by $1/\omega_0$); hidden sine layers $\mathbf{W}_i \sim \mathcal{U}(-\sqrt{6/n}/\omega, \sqrt{6/n}/\omega)$ with $n = 256$. The SDF output is initialized near zero ($\pm 10^{-5}$). ReLU layers in the segmentation head use Kaiming initialization; the final classifier is initialized in $\pm 10^{-3}$ so logits start nearly uniform.

Training configuration. We use Adam with learning rate 5×10^{-5} , batch size 1 (one shape per iteration), and 10 epochs. Loss weights are $\lambda_{\text{DM}}=7000$, $\lambda_{\text{DNM}}=600$, $\lambda_{\text{eik}}=50$, $\lambda_{\text{ODW}}=10$, $\lambda_{\text{seg}}=100$. The segmentation loss is applied only to labeled manifold samples; geometric losses follow the manifold/non-manifold split.

Segmentation heads. Four classifier variants are evaluated with the same SDF trunk: (i) ReLU: two ReLU layers (with dropout) then linear; (ii) SIREN: two sine layers (first with large ω_0) then linear; (iii) Hybrid: one sine layer followed by ReLU layers; (iv) Deep_skip: a deeper sine stack with skip connections from the input and an early hidden layer.

Mesh extraction. Meshes are extracted with Marching Cubes on a fixed 256^3 grid over the normalized training volume at the zero level set. SDF queries are chunked to control memory. Vertices (in voxel-index space) are mapped to network space and then to world coordinates via the same normalization; per-vertex labels are obtained by evaluating the segmentation head at *normalized* vertex positions, and each face takes the majority label of its three vertices. Visualizations may use arbitrary color palettes; evaluation uses label metrics (mean Intersection over Union, accuracy, segmentation consistency).

4 Experiments and Results

We evaluate on randomly selected meshes from the ABC dataset, with per-face labels generated automatically using PartField. Over-segmentation is intentionally allowed on some shapes to test robustness to varying part counts. PartField is used only for supervision; inference uses our network without PartField components. The test set spans 2–18 parts.

For each test mesh, we load the ground-truth point cloud and labels from the provided .ply file, and sample the same number of points on the predicted mesh surface. All metrics are computed per shape and reported as mean \pm standard deviation across the set.

Reconstruction is evaluated following FlatCAD, using Chamfer distance (CD_{L1} and CD_{L2}) computed over bidirectional nearest neighbours, normal consistency (NC) as the mean cosine similarity of matched normals, and micro-averaged $F1_\mu$ at the FlatCAD threshold. Segmentation accuracy (Acc.) is measured by transferring ground-truth labels to predicted samples via nearest neighbour in 3D, computing per-part IoU, aggregating to mean Intersection over Union (mIoU), and reporting per-point accuracy.

We also introduce a segmentation consistency (Consis.) metric. For predicted samples $P = \{(x_i, \ell_i)\}$, we use $\mathbf{1}[\ell_j = \ell_i]$ the indicator function to compute

$$c_i = \frac{1}{k} \sum_{j \in \mathcal{N}_k(x_i)} \mathbf{1}[\ell_j = \ell_i],$$

with $k = 10$, and average c_i over $M = \min(1000, |P|)$ anchors. This measures local label smoothness in prediction space and is invariant to palette permutations. Finally, we record the number of predicted and ground-truth parts for each shape.

4.1 Results

Table 1 shows comparison to FlatCAD. We compare four segmentation heads (ReLU, SIREN, Hybrid, Deep_skip). On the same 20 shapes, SIREN/Hybrid/Deep-skip show no significant changes in CD, NC, or $F1$ ($\Delta \approx 0$, paired t-tests $p > 0.05$), indicating the head is plug-in and reconstruction-neutral; ReLU trends slightly worse.

Table 2 reports the reconstruction and corresponding segmentation mean \pm std over 50 randomly selected shapes. Lower is better for CD_{L1}/CD_{L2} ; higher is better for $F1_\mu$, NC, mIoU, Acc. and Consis. All methods achieve strong reconstruction accuracy. SIREN attains the lowest Chamfer distances, closely followed by Hybrid. Hybrid reaches the best $F1_\mu$ and NC, with SIREN a close second. Segmentation accuracy is uniformly high: mIoU ≥ 0.951 , per-point accuracy ≥ 0.971 , and segmentation consistency ≥ 0.966 . Among models, Hybrid yields the highest mIoU (0.967), while SIREN achieves the best accuracy (0.978) and the highest consistency (0.973).

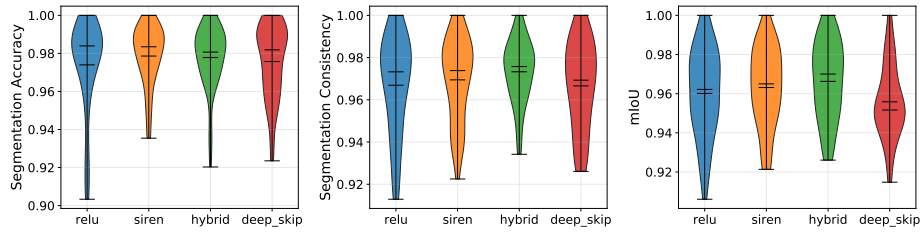


Fig. 2: Model comparison across segmentation metrics (colors indicate model types).

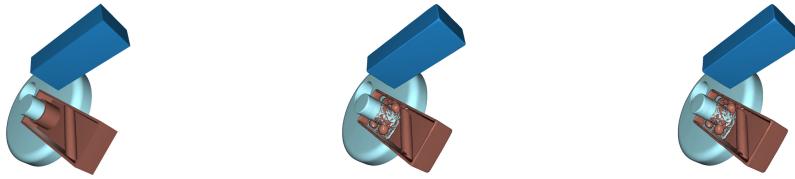


Fig. 3: Failure case: GT vs. Hybrid vs. SIREN. The reconstructed meshes are imperfect, yet segmentations remain coherent (correct part count and high consistency).

Breakdowns by part count show consistent behavior: differences between SIREN and Hybrid remain small, and both clearly outperform ReLU and Deep_skip. Table 3 presents per-part mIoU (\pm standard deviation). Columns P_k correspond to part label k . Beyond per-metric comparisons, we analyze correlations between reconstruction and segmentation metrics (Table 4). Overall, SIREN achieves the lowest Chamfer distances and highest per-point accuracy/consistency, while Hybrid provides the best mIoU and $F1_{\mu}/NC$. This demonstrates that the proposed framework yields accurate reconstructions with semantically stable segmentations across a range of part counts.

Figure 2 depicts results across reconstruction and segmentation metrics. Figure 4 shows visual comparisons.

4.2 Limitations

Although the method handles meshes with arbitrary part counts and maintains segmentation stability even with imperfect reconstructions, fine-grained boundary segmentation remains a challenge. We observe occasional leaks or frayed borders in thin structures and at tight fillets (see Fig. 3). This comes from the supervision source: PartField provides per-face labels on meshes of varying tessellation quality, so boundaries inherit face-scale discretization. Higher resolution supervision would mitigate this.

5 Conclusions

We presented a joint implicit framework for CAD surface reconstruction and part segmentation by extending FlatCAD with a segmentation head. The approach leverages shared SIREN features to predict both signed distance values and per-part labels in a unified representation. Experiments on PartField-supervised ABC meshes demonstrate that the method achieves strong reconstruction accuracy while delivering high segmentation performance, with mIoU above 0.96 and accuracy above 0.97 across diverse part

Table 1: Reconstruction on 20 random shapes. Δ is head-FlatCAD (CD: lower is better; NC/F1 $_{\mu}$: higher).

model	CD $_{L1}$		NC		F1 $_{\mu}$	
	mean \pm std	Δ	mean \pm std	Δ	mean \pm std	Δ
FlatCAD	0.42 \pm 0.31	—	0.953 \pm 0.042	—	0.849 \pm 0.127	—
ReLU	0.57 \pm 0.47	+0.001489	0.939 \pm 0.062	-0.0138	0.762 \pm 0.269	-0.0871
SIREN	0.42 \pm 0.28	+0.000006	0.955 \pm 0.044	+0.0016	0.834 \pm 0.143	-0.0150
Hybrid	0.42 \pm 0.28	+0.000009	0.955 \pm 0.044	+0.0019	0.835 \pm 0.143	-0.0149
Deep_skip	0.45 \pm 0.36	+0.000361	0.952 \pm 0.048	-0.0017	0.830 \pm 0.163	-0.0192

Table 2: Main results. See Sec. 4 for metric definitions.**(a) Reconstruction**

model_type	N	CD $_{L1}$ ($\times 10^{-2}$)	CD $_{L2}$ ($\times 10^{-2}$)	NC	F1 $_{\mu}$
ReLU	50	0.59 \pm 1.30	0.05 \pm 0.21	0.94 \pm 0.07	0.78 \pm 0.28
SIREN	50	0.51 \pm 0.89	0.04 \pm 0.12	0.95 \pm 0.06	0.82 \pm 0.17
Hybrid	50	0.49 \pm 0.95	0.03 \pm 0.11	0.95 \pm 0.06	0.83 \pm 0.15
Deep_skip	50	0.62 \pm 0.65	0.03 \pm 0.13	0.95 \pm 0.06	0.82 \pm 0.19

(b) Segmentation

model_type	N	mIoU	Acc.	Consis.
ReLU	50	0.96 \pm 0.02	0.97 \pm 0.02	0.97 \pm 0.02
SIREN	50	0.96 \pm 0.02	0.98 \pm 0.01	0.97 \pm 0.02
Hybrid	50	0.97 \pm 0.01	0.98 \pm 0.02	0.97 \pm 0.01
Deep_skip	50	0.95 \pm 0.02	0.98 \pm 0.02	0.97 \pm 0.02

counts. A paired comparison with FlatCAD shows *no significant differences* in reconstruction, indicating that the head is plug-in and reconstruction-neutral. Our proposed segmentation consistency metric further confirms label coherence even under imperfect reconstructions. Because the head is decoupled from the SDF trunk, it can be attached to *existing* SDF-based reconstruction models with minimal effort.

References

1. Atzmon, M., Lipman, Y.: Sal: Sign agnostic learning of shapes from raw data. 2020 IEEE/CVF Conference on Computer Vision and Pattern Recognition (CVPR) (2020)
2. Atzmon, M., Lipman, Y.: Sal++: Sign agnostic learning with derivatives. ArXiv [abs/2006.05400](#) (2020)
3. Ben-Shabat, Y., Koneputugodage, C.P.H., Gould, S.: Digs : Divergence guided shape implicit neural representation for unoriented point clouds. 2022 IEEE/CVF Conference on Computer Vision and Pattern Recognition (CVPR) pp. 19301–19310 (2022)
4. Chabra, R., Lenssen, J.E., Ilg, E., Schmidt, T., Straub, J., Lovegrove, S., Newcombe, R.A.: Deep local shapes: Learning local sdf priors for detailed 3d reconstruction. In: European Conference on Computer Vision (2020)

Table 3: Per-part IoU on 50 shapes (mean \pm std). Columns P_k correspond to part label k .

(a) P_0 – P_8									
model_type	P0	P1	P2	P3	P4	P5	P6	P7	P8
ReLU	0.93 \pm 0.20	0.94 \pm 0.12	0.94 \pm 0.12	0.93 \pm 0.17	0.90 \pm 0.23	0.89 \pm 0.24	0.88 \pm 0.22	0.89 \pm 0.15	0.92 \pm 0.09
SIREN	0.94 \pm 0.17	0.94 \pm 0.15	0.94 \pm 0.16	0.93 \pm 0.13	0.95 \pm 0.14	0.90 \pm 0.28	0.91 \pm 0.20	0.92 \pm 0.15	0.98 \pm 0.01
Hybrid	0.94 \pm 0.14	0.93 \pm 0.17	0.96 \pm 0.12	0.97 \pm 0.08	0.97 \pm 0.10	0.95 \pm 0.13	0.94 \pm 0.18	0.92 \pm 0.16	0.99 \pm 0.02
Deep_skip	0.94 \pm 0.14	0.94 \pm 0.14	0.95 \pm 0.11	0.94 \pm 0.12	0.95 \pm 0.14	0.89 \pm 0.24	0.90 \pm 0.16	0.91 \pm 0.18	0.98 \pm 0.01

(b) P_9 – P_{17}									
model_type	P9	P10	P11	P12	P13	P14	P15	P16	P17
ReLU	0.89 \pm 0.03	0.92 \pm 0.07	0.88 \pm 0.17	0.99 \pm 0.00	0.72 \pm 0.15	0.99 \pm 0.00	0.99 \pm 0.00	0.98 \pm 0.00	0.99 \pm 0.00
SIREN	0.91 \pm 0.09	0.94 \pm 0.08	0.92 \pm 0.14	0.94 \pm 0.06	0.75 \pm 0.14	0.98 \pm 0.00	0.99 \pm 0.00	0.99 \pm 0.00	0.98 \pm 0.00
Hybrid	0.95 \pm 0.07	0.99 \pm 0.01	0.96 \pm 0.09	0.99 \pm 0.01	0.90 \pm 0.07	0.99 \pm 0.00	0.99 \pm 0.00	0.99 \pm 0.00	0.99 \pm 0.00
Deep_skip	0.85 \pm 0.11	0.93 \pm 0.02	0.91 \pm 0.17	0.96 \pm 0.04	0.81 \pm 0.07	0.98 \pm 0.00	0.98 \pm 0.00	0.98 \pm 0.00	0.98 \pm 0.00

Table 4: Correlation (Pearson r) between reconstruction metrics and segmentation metrics. Negative values for CD_{L1} indicate that lower Chamfer distances correlate with higher segmentation scores; correlations with Consis. are weak, suggesting robustness to geometric errors.

	Overall	ReLU	SIREN	Hybrid	Deep_skip
$CD_{L1} \leftrightarrow mIoU$	-0.68	-0.74	-0.77	-0.68	-0.77
$CD_{L1} \leftrightarrow Acc.$	-0.76	-0.78	-0.82	-0.67	-0.85
$CD_{L1} \leftrightarrow Consis.$	0.08	-0.12	-0.13	-0.06	-0.19
$NC \leftrightarrow mIoU$	0.23	0.27	0.27	0.19	0.20
$NC \leftrightarrow Acc.$	0.25	0.28	0.26	0.22	0.19
$NC \leftrightarrow Consis.$	0.13	0.10	0.24	0.03	0.16
$F1_\mu \leftrightarrow mIoU$	0.48	0.65	0.38	0.41	0.40
$F1_\mu \leftrightarrow Acc.$	0.57	0.73	0.54	0.59	0.56
$F1_\mu \leftrightarrow Consis.$	0.10	0.18	0.11	0.09	0.07

- Chen, Z., Yin, K., Fisher, M., Chaudhuri, S., Zhang, H.: Bae-net: Branched autoencoder for shape co-segmentation. In: Proceedings of the IEEE/CVF International Conference on Computer Vision. pp. 8490–8499 (2019)
- Chibane, J., Alldieck, T., Pons-Moll, G.: Implicit functions in feature space for 3d shape reconstruction and completion. 2020 IEEE/CVF Conference on Computer Vision and Pattern Recognition (CVPR) pp. 6968–6979 (2020)
- Dong, Q., Xu, R., Wang, P., Chen, S., Xin, S., Jia, X., Wang, W., Tu, C.: Neurcadrecon: Neural representation for reconstructing cad surfaces by enforcing zero gaussian curvature. ACM Transactions on Graphics (TOG) **43**, 1 – 17 (2024)
- Erler, P., Guerrero, P., Ohrhallinger, S., Mitra, N.J., Wimmer, M.: Points2surf learning implicit surfaces from point clouds. In: European Conference on Computer Vision (2020)
- Fan, S., Musialski, P.: Optimizing 3d geometry reconstruction from implicit neural representations. In: 2024 International Conference on Machine Learning and Applications (ICMLA). pp. 816–821 (2024)
- Gropp, A., Yariv, L., Haim, N., Atzmon, M., Lipman, Y.: Implicit geometric regularization for learning shapes. In: International Conference on Machine Learning (2020)

11. Koch, S., Matveev, A., Jiang, Z., Williams, F., Artemov, A., Burnaev, E., Alexa, M., Zorin, D., Panozzo, D.: Abc: A big cad model dataset for geometric deep learning. In: The IEEE Conference on Computer Vision and Pattern Recognition (CVPR) (June 2019)
12. Liu, L., Wang, B., Xie, H., Liu, D., Liu, L., Tian, Z., Yang, K., Wang, B.: Surroundsdf: Implicit 3d scene understanding based on signed distance field. 2024 IEEE/CVF Conference on Computer Vision and Pattern Recognition (CVPR) pp. 21614–21623 (2024)
13. Liu, M., Uy, M.A., Xiang, D., Su, H., Fidler, S., Sharp, N., Gao, J.: Partfield: Learning 3d feature fields for part segmentation and beyond. ArXiv **abs/2504.11451** (2025)
14. Mescheder, L.M., Oechsle, M., Niemeyer, M., Nowozin, S., Geiger, A.: Occupancy networks: Learning 3d reconstruction in function space. 2019 IEEE/CVF Conference on Computer Vision and Pattern Recognition (CVPR) pp. 4455–4465 (2019)
15. Müller, T., Evans, A., Schied, C., Keller, A.: Instant neural graphics primitives with a multiresolution hash encoding. ACM Transactions on Graphics (TOG) **41**, 1 – 15 (2022)
16. Park, J.J., Florence, P.R., Straub, J., Newcombe, R.A., Lovegrove, S.: Deepsdf: Learning continuous signed distance functions for shape representation. 2019 IEEE/CVF Conference on Computer Vision and Pattern Recognition (CVPR) pp. 165–174 (2019)
17. Peng, S., Niemeyer, M., Mescheder, L.M., Pollefeys, M., Geiger, A.: Convolutional occupancy networks. ArXiv **abs/2003.04618** (2020)
18. Qi, C., Yi, L., Su, H., Guibas, L.J.: Pointnet++: Deep hierarchical feature learning on point sets in a metric space. In: NIPS (2017)
19. Schnabel, R., Wahl, R., Klein, R.: Efficient ransac for point-cloud shape detection. Computer Graphics Forum **26**(2), 214–226 (2007)
20. Shlafman, S., Tal, A., Katz, S.: Metamorphosis of polyhedral surfaces using decomposition. Computer Graphics Forum **21**(3), 219–228 (2002)
21. Sidi, O., van Kaick, O., Kleiman, Y., Zhang, H., Cohen-Or, D.: Unsupervised co-segmentation of a set of shapes via descriptor-space spectral clustering. In: ACM Transactions on Graphics (TOG). vol. 30, pp. 1–10 (2011)
22. Sitzmann, V., Martel, J.N., Bergman, A.W., Lindell, D.B., Wetzstein, G.: Implicit neural representations with periodic activation functions. In: Proc. NeurIPS (2020)
23. Talabot, N., Clerc, O., Demirtas, A.C., Oner, D., Fua, P.: Partsdf: Part-based implicit neural representation for composite 3d shape parametrization and optimization. ArXiv **abs/2502.12985** (2025)
24. Uy, M.A., Chang, Y.Y., Sung, M., Goel, P., Lambourne, J., Birdal, T., Guibas, L.J.: Point2cyl: Reverse engineering 3d objects from point clouds to extrusion cylinders. 2022 IEEE/CVF Conference on Computer Vision and Pattern Recognition (CVPR) pp. 11840–11850 (2021)
25. Wang, Z., Zhang, Y., Xu, R., Zhang, F., Wang, P., Chen, S., Xin, S., Wang, W., Tu, C.: Neural-singular-hessian: Implicit neural representation of unoriented point clouds by enforcing singular hessian. ACM Transactions on Graphics (TOG) **42**, 1 – 14 (2023)
26. Wu, Q., Liu, X., Chen, Y., Li, K., Zheng, C., Cai, J., Cai, J.: Objectsdf: Object-compositional neural implicit surfaces. In: European Conference on Computer Vision. pp. 197–213 (2022)
27. Wu, Q., Wang, K., Li, K., Zheng, J., Cai, J.: Objectsdf++: Improved object-compositional neural implicit surfaces. arXiv preprint arXiv:2308.07868 (2023)
28. Wu, T., Zheng, C., Cham, T.J., Wu, Q.: Clusteringsdf: Self-organized neural implicit surfaces for 3d decomposition. In: European Conference on Computer Vision (2024)
29. Ye, J., Chen, Y., Wang, N., Wang, X.: Gifs: Neural implicit function for general shape representation. 2022 IEEE/CVF Conference on Computer Vision and Pattern Recognition (CVPR) pp. 12819–12829 (2022)
30. Yin, H., Plocharski, A., Włodarczyk, M.J., Kida, M., Musialski, P.: FlatCAD: Fast Curvature Regularization of Neural SDFs for CAD Models. Computer Graphics Forum (Proc. Pacific Graphics) **44** (7) (2025)

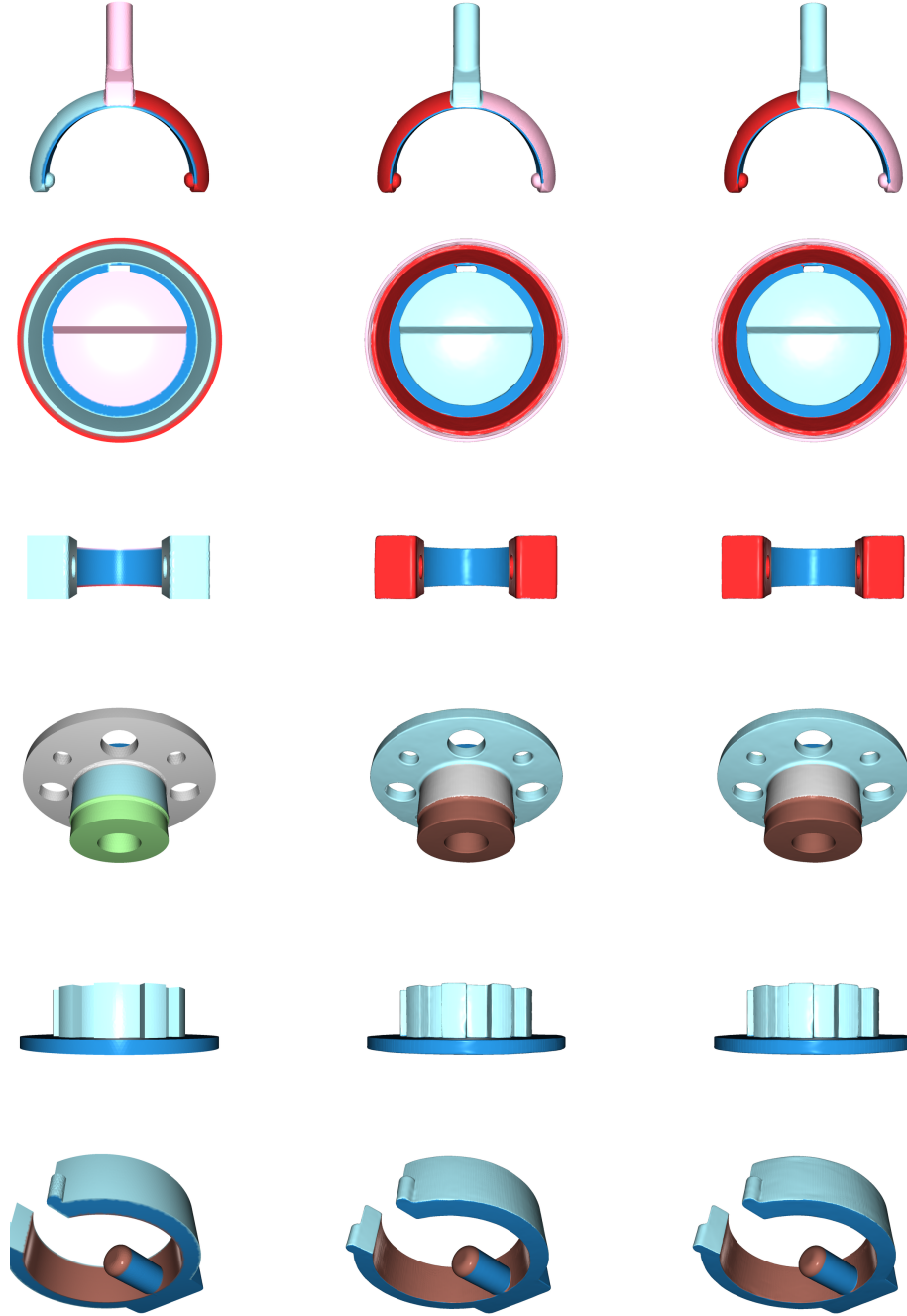


Fig. 4: GT vs. Hybrid vs. SIREN qualitative comparison. Colors may differ from the original PartField palette (palette permutations), but *part identities* are evaluated by labels (mIoU/Acc./Consis.), not RGB.